JOC Article

Allene as the Parent Substrate in Zinc-Mediated Biomimetic Hydration Reactions of Cumulenes†

Burkhard O. Jahn, Wilhelm A. Eger, and Ernst Anders*

Institut of Organic and Macromolecular Chemistry, Friedrich Schiller University Jena, Humboldtstrasse 10, 07743 Jena, Germany

ernst.anders@uni-jena.de

Received June 26, 2008

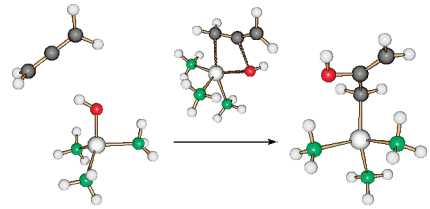

The aim of our present investigation is to unravel the general mode of biomimetic activation of a wide variety of cumulenes by carbonic anhydrase (CA) models. Carbonic anhydrases allow the specific recognition, activation and transfer not only of CO_2 but also of heteroallenes X=C=Y such as the polar or polarizable examples COS, CS_2, H_2CCO, and RNCS. Therefore, this enzyme class fulfils the requirements of excellent catalysts with a wide variety of important applications. Can this be extended to the isoelectronic but less reactive allene molecule, $H_2C{=}C{=}CH_2$ and extremely simplified models as mimetic concept for active center of the carbonic anhydrase? Allene is a waste product in the refinery, i.e. the C3-cut of the naphtha distillation; therefore, any addition product that can be obtained from allene in high yields will be of significant value. We investigated the complete catalytic cycle of a very simple model reaction, the hydration of allene, using density functional theory. Additionally, calculations were performed for the uncatalyzed reaction. There are two possible ways for the nucleophilic attack leading to different products. The zinc hydroxide complex and the water molecule can react at the central or the terminal carbon atoms (positional selecticity), the resulting products are 2-propen-1-ol and propen-2-ol, respectively, acetone. The calculations indicate a significant lower energy barrier for the rate determining step of the formation of propen-2-ol and therefore a well-expressed regioselectivity for the addition of such small molecules. The zinc complex has a pronounced catalytic effect and lowers the activation barrier from 262.5 to 123.9 kJ/mol compared with the uncatalyzed reaction. This work suggests the most probable paths for this reaction and discloses the necessity for the development of novel catalysts.

Introduction

Carbonic anhydrases, a ubiquitous family of zinc enzymes, catalyze the hydration of the heterocumulene carbon dioxide to carbonic acid. This reaction is important for physiological processes in all living organisms, such as respiration, photosynthesis, or acid−base balance. Human carbonic anhydrase HCA II, which is the most efficient one, accelerates this hydration by a factor of 10^7.[1,2] Thus it is possible to remove the excessive CO_2 continuously from organisms to the surrounding atmosphere. In the active site of HCA II, a single Zn^{2+} cation is surrounded by three imidazole ligands originating from three histidyl side chains. Depending on the pH value, the central metal ion coordinates water or a hydroxide ion.[3] This fundamental reaction has led to an intense and continuing research for structure details and the mode of action.[4−10]

Carbon dioxide and propadiene (allene) are isoelectronic. Therefore it is conceivable that there could be a variety of possibilities which allow the zinc mediated hydration of this cumulene analog to the natural prototype. The general aim of this work is the density functional theory (DFT) based and experimental search for such biomimetic reaction paths in which allenes play the role of the natural cumulene, CO_2. This can be

† Dedicated to Professor Dr. Alan R. Katritzky on the occasion of his 80th birthday.

(1) Lindskog, S. *Pharmacol. Ther.* **1997**, *74*, 1–20.
(2) Liang, J.-Y.; Lipscomb, W. N. *J. Am. Chem. Soc.* **1986**, *108*, 5051–5058.
(3) Håkansson, K.; Carlsson, M.; Svensson, L. A.; Liljas, A. *J. Mol. Biol.* **1992**, *227*, 1192–1204.

10.1021/jo801358m CCC: $40.75
Published on Web 10/11/2008

of synthetic and commercial interest, vide infra. So far hydrogenation dominates in the industrial research.[11−17]

The catalytic cycle of the CO_2 hydration was investigated with the so-called ammonia model, the simplest biomimetic theoretical model for the elaborate enzyme.[4,18] The zinc atom is complexed by three ammonia molecules and a hydroxide ion. So it is possible to calculate all kinds of reaction paths at an acceptable high theoretical level which allows the estimation of very reliable energy relationships and structural predictions.

Allene is the simplest cumulated hydrocarbon. Since van't Hoff has predicted the correct structures of allene and higher cumulenes, chemists are fascinated by the extraordinary properties like axial chirality of the elongated tetrahedron if two different substituents at every terminal carbon exist.[19] Even cyclic allenes were synthesized.[20] Allene with its isomer methyl acetylene accrues in large amounts in the C3-cut of the naphtha distillation. Both compounds are hydrogenated to propene.[21] About 150 biogenic compounds with inclusion of allenic systems are known. They have different biological functions and the chirality of different substituted allenes probably plays a relevant role. For example, a nongenetically coded allenic amino acid is known.[22] Hints for an activity of mixtures containing allene and zinc compounds came from Temkin et al.[23] Allene with methanol on zinc oxide and zinc nitrate spread out on charcoal or silica gel in the gas phase yielded to 2-methoxypropene. Teles et al. could not verify all of these results.[24] They found only an activity on silicagel with zinc acetate in methanol and obtained 2-methoxypropene and 2,2-dimethoxypropene in 85% yield.

The present work is focused to investigate the possibility for a CO_2 analog reaction of allene with carbonic anhydrase (CA) models. The aim is to set the basics for development of new catalysts. For this reason all conceivable kinds of pathways were investigated. This is therefore the first report with the complete description of a zinc complex catalyzed allene hydration inclusive the consecutive reactions. Some analogous aspects of comparable reactions with the cumulens ketene and CO_2 are included in the discussion. This investigation is an example for our general research topic *Metal Mediated Activation of Organic Compounds Modeled after Nature*.[25]

Computational Methods

All structure and energy calculations were performed using the mPW1k functional (modified Perdew−Wang 1-parameter for kinetics)[26] in combination with the augmented cc-pVDZ basis set.[27−29] The hybrid density mPW1k functional is a modified PW91 functional for kinetics and the calculation of energy barriers. It is based on the Perdew−Wang exchange functional[30] with Adamo and Barone's modified enhancement factor[31] and the Perdew−Wang correlation functional.[30] A larger percentage of Hartree−Fock exchange has been introduced to circumvent the underestimated barrier heights typical of standard exchange-correlation functionals. It has been shown that this functional generally yields much more

(4) Bräuer, M.; Pérez-Lustres, J. L.; Weston, J.; Anders, E. *Inorg. Chem.* **2002**, *41*, 1454–1463.
(5) Bottoni, A.; Lanza, C. Z.; Miscione, G. P.; Spinelli, D. *J. Am. Chem. Soc.* **2004**, *126*, 1542–1550.
(6) Fisher, S.; Maupin, C.; Budayova-Spano, M.; Govindasamy, L.; Tu, C.; Agbandje-McKenna, M.; Silverman, D.; Voth, G.; McKenna, R. *Biochemistry* **2007**, *46*, 2930–2937.
(7) Maupin, C.; Voth, G. *Biochemistry* **2007**, *46*, 2938–2947.
(8) Sousa, S.; Fernandes, P.; Ramos, M. *J. Am. Chem. Soc.* **2007**, *129*, 1378–1385.
(9) Hartmann, M.; Clark, T.; van Eldik, R. *J. Mol. Model.* **1996**, *2*, 358–361.
(10) Hartmann, M.; Merz, K. M., Jr.; van Eldik, R.; Clark, T. *J. Mol. Model.* **1998**, *4*, 355–365.
(11) Hatscher, S.; Hesse, M. *Process for hydrogenating unsaturated hydrocarbons in the presence of catalysts containing copper and zinc*. Patent WO 2008009568 (A1), 2008.
(12) Dai, W.; Fang, Y.; Li, D.; Kuang, C.; Liu, Z.; Cheng, H.; Cheng, J.; Wang, F.; Liao, L.; Xing, Y.; Gu, L.; Guo, H. *Preparation of catalyst for selective hydrogenation of alkyne and diene*. Patent CN 101062483 (A), 2007.
(13) Dai, W.; Wei, G.; Peng, H.; Mu, W.; Fang, Y.; Liu, H.; Qi, W.; Lu, H.; He, G.; Guo, Y.; Zhu, J. *Manufacture and application of catalyst for selective hydrogenation of alkynes and dienes*. Patent CN 1958155 (A), 2007.
(14) Wang, J.; Liu, Q.; Shi, Y.; Nie, H.; Li, D.; Dai, L.; Hu, Y.; Kang, X.; Jia, S. , *Selective hydrogenation catalyst for removing allenes and its preparation*. Patent CN 1827746 (A), 2006.
(15) Dong, M.; Zong, B.; Zhang, X.; Meng, X.; Mu, X.; Pan, Z. *Selective hydrogenation method for alkyne or diolefin with amorphous alloy catalyst*. Patent CN 1631859 (A), 2005.
(16) Li, M.; Chu, Y.; Hu, Y.; Xia, G.; Nie, H.; Shi, Y.; Li, D.; Zhang, R.; Zhu, M. *Method for removing allenes from distillate oil by selective hydrogenation*. Patent CN 1676582 (A), 2005.
(17) Li, M.; Chu, Y.; Hu, Y.; Xia, G.; Nie, H.; Shi, Y.; Li, D.; Zhang, R.; Zhu, M. *Method for removing allenes from distillate oil by selective hydrogenation*. Patent CN 1676580 (A), 2005.
(18) Mauksch, M.; Bräuer, M.; Weston, J.; Anders, E. *ChemBioChem* **2001**, *2*, 190–198.
(19) van't Hoff, J. H. *La Chimie dans L'Espace*; Bazendijk: Rotterdam, 1875; Vol. 1.
(20) Wentrup, C.; Gross, G.; Maquestiau, A.; Flammang, R. *Angew. Chem.* **1983**, *95*, 551.
(21) DiTusa, C. A.; Christensen, T.; McCall, K. A.; Fierke, C. A.; Toone, E. J. Isomerisierung von Propadien zu Methylacetylen, http://forkat.anorg.chemie.tu-muenchen.de/biblio/texte/pdf/f2be00c7.pdf, accessed September 17, 2008.
(22) Hoffmann-Röder, A.; Krause, N. *Angew. Chem.* **2004**, *116*, 1216–1236.
(23) Temkin, O. N.; Sestakov, G.; Kuprijanova, L.; Taber, A.; Zukovskij, S.; Agre, V.; Sorokin, B. A.; Zavorotov, V.; Pinchasik, E.; Vasserberg, V. *Chem. Abstr*, **1990**, *112*, 54987b.
(24) Breuer, K.; Teles, J. H.; Demuth, D.; Hibst, H.; Schäfer, A.; Brode, S.; Domgörgen, H. *Angew. Chem.* **1999**, *111*, 1497–1502.
(25) Metal Mediated Reactions Modeled after Nature was the general topic of a Collaborative Research Center at the University of Jena, Germany (1997-2006), sponsored by the Deutsche Forschungsgemeinschaft, Germany.
(26) Lynch, B.; Fast, P.; Harris, M.; Truhlar, D. *J. Phys. Chem. A* **2000**, *104*, 4811–4815.
(27) Dunning, T. H., Jr *J. Chem. Phys.* **1989**, *90*, 1007–1023.
(28) Kendall, R. A.; Dunning, T. H., Jr.; Harrison, R. J. *J. Chem. Phys.* **1992**, *96*, 6796–6806.
(29) Wiberg, K. B. *J. Comput. Chem.* **2004**, *25*, 1342–1346.
(30) Perdew, J. P.; Chevary, J.; Vosko, S.; Jackson, K. A.; Peterson, M. R.; Singh, D.; Fiolhais, C. *Phys. Rev. B* **1992**, *46*, 6671.
(31) Adamo, C.; Barone, V. *J. Chem. Phys.* **1998**, *108*, 664–675.
(32) Lynch, B.; Truhlar, D. *J. Phys. Chem. A* **2001**, *105*, 2936–2941.
(33) Lynch, B.; Truhlar, D. *J. Phys. Chem. A* **2002**, *106*, 842–846.
(34) Gilbert, T. M. *J. Phys. Chem. A* **2004**, *108*, 2550–2554.
(35) Lingwood, M.; Hammond, J.; Hrovat, D.; Mayer, J.; Borden, W. *J. Chem. Theory Comput.* **2006**, *2*, 740–745.
(36) Frisch, M. J.; Trucks, G. W.; Schlegel, H. B.; Scuseria, G. E.; Robb, M. A.; Cheeseman, J. R.; Zakrzewski, V. G.; Montgomery, J. A., Jr.; Stratmann, R. E.; Burant, J. C.; Dapprich, S.; Millam, J. M.; Daniels, A. D.; Kudin, K. N.; Strain, M. C.; Farkas, O.; Tomasi, J.; Barone, V.; Cossi, M.; Cammi, R.; Mennucci, B.; Pomelli, C.; Adamo, C.; Clifford, S.; Ochterski, J.; Petersson, G. A.; Ayala, P. Y.; Cui, Q.; Morokuma, K.; Rega, N.; Salvador, P.; Dannenberg, J. J.; Malick, D. K.; Rabuck, A. D.; Raghavachari, K.; Foresman, J. B.; Cioslowski, J.; Ortiz, J. V.; Baboul, A. G.; Stefanov, B. B.; Liu, G.; Liashenko, A.; Piskorz, P.; Komaromi, I.; Gomperts, R.; Martin, R. L.; Fox, D. J.; Keith, T.; Al-Laham, M. A.; Peng, C. Y.; Nanayakkara, A.; Challacombe, M.; Gill, P. M. W.; Johnson, B.; Chen, W.; Wong, M. W.; Andres, J. L.; Gonzalez, C.; Head-Gordon, M.; Replogle, E. S.; Pople, J. A. *Gaussian98*; Gaussian, Inc.: Wallingford, CT, 2002; http://www.gaussian.com.
(37) Frisch, M. J.; Trucks, G. W.; Schlegel, H. B.; Scuseria, G. E.; Robb, M. A.; Cheeseman, J. R.; Montgomery, J. A., Jr.; Vreven, T.; Kudin, K. N.; Burant, J. C.; Millam, J. M.; Iyengar, S. S.; Tomasi, J.; Barone, V.; Mennucci, B.; Cossi, M.; Scalmani, G.; Rega, N.; Petersson, G. A.; Nakatsuji, H.; Hada, M.; Ehara, M.; Toyota, K.; Fukuda, R.; Hasegawa, J.; Ishida, M.; Nakajima, T.; Honda, Y.; Kitao, O.; Nakai, H.; Klene, M.; Li, X.; Knox, J. E.; Hratchian, H. P.; Cross, J. B.; Adamo, C.; Jaramillo, J.; Gomperts, R.; Stratmann, R. E.; Yazyev, O.; Austin, A. J.; Cammi, R.; Pomelli, C.; Ochterski, J. W.; Ayala, P. Y.; Morokuma, K.; Voth, G. A.; Salvador, P.; Dannenberg, J. J.; Zakrzewski, V. G.; Dapprich, S.; Daniels, A. D.; Strain, M. C.; Farkas, O.; Malick, D. K.; Rabuck, A. D.; Raghavachari, K.; Foresman, J. B.; Ortiz, J. V.; Cui, Q.; Baboul, A. G.; Clifford, S.; Cioslowski, J.; Stefanov, B. B.; Liu, G.; Liashenko, A.; Piskorz, P.; Komaromi, I.; Martin, R. L.; Fox, D. J.; Keith, T.; Al-Laham, M. A.; Peng, C. Y.; Nanayakkara, A.; Challacombe, M.; Gill, P. M. W.; Johnson, B.; Chen, W.; Wong, M. W.; Gonzalez, C.; Pople, J. A. *Gaussian03*; Gaussian, Inc.: Wallingford, CT, 2004; http://www.gaussian.com.

TABLE 1. Charge Distribution from the NPA for Allene, Carbon Dioxide, and Ketene Segregated and in the Transition States with the Zinc Hydroxide Complex As Well As for Water and the Segregated Zinc Hydroxide Complex 5

molecule[a]	atom	natural charge
allene	C terminal	−0.511
	C central	0.071
7(ts); *123.9*	C central	0.226
	C Zn-bound	−0.912
	C extroverted	−0.462
carbon dioxide	C	1.127
	O	−0.567
TS (CO_2 + **5**); *55.6*[b]	C	1.136
	O Zn-bound	−0.787
	O extroverted	−0.593
ketene	C terminal	−0.818
	C central	0.768
	O	−0.496
TS (H_2CCO + **5**); *75.9*[c]	C central	0.912
(CC attack)	C Zn-bound	−1.119
	O extroverted	−0.416
TS (H_2CCO + **5**); *36.6*[c]	C central	0.735
(CO attack)	O Zn-bound	−0.705
	C extroverted	−0.716
water	O	−0.982
	H	0.491
5	O	−1.379
	H O-bound	0.505

[a] $\Delta\Delta G_a$ [kJ/mol], activation energy in italics. [b] Starting the geometry taken from ref 18 and reoptimized at mPW1k/aug-cc-pVDZ. [c] Starting geometry adapted to **7(ts)** respectively the CO_2 TS, level of theory mPW1k/aug-cc-pVDZ.

reliable reaction barrier heights than B3LYP.[26,32−35] All calculations were realized by using the Gaussian 98[36] and Gaussian 03[37] program packages. NBO analyses were performed by using NBO 5.0.[38] Stable structure geometries were characterized by frequency calculation. The structures represent energetic minima without the existence of imaginary modes. One imaginary frequency characterizes a transition state. The visualization of this mode illustrates the reaction path. Ambiguous TS were verified by IRC[39,40] or BOMD[41,42] calculations. Solvent corrections were performed as CPCM single point calculations[43−45] in methanol with the same method and basis set as for the gas phase calculations. Methanol was used due to its protic and polar properties. Optimization of the ammonia model is impossible in solvents.[46] The solvent corrected energies are significantly higher than the gas phase energies. The variance is roughly 50 kJ/mol for the zinc catalyzed reaction and 20 kJ/mol for the uncatalyzed as well as the water catalyzed reactions. This does not result in modifications of the relative energies. Solvent corrected and gas phase barriers differ by only about 10 kJ/mol. For details, see the Supporting Information and Table 2. All energy values termed in the text and figures are the optimized gas phase energies.

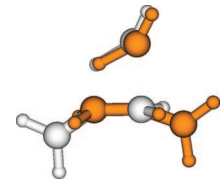

FIGURE 1. Superimposed structures of **3(ts)** (brown) and **3a(ts)** (gray) (in the case of substituted allenes, this is an example for positional selectivity).

TABLE 2. Gibbs Free Energy Values and Activation Barriers Relative to the Separated Reactants Allene and Water for the Uncatalyzed and Water Catalyzed Reaction Paths, Respectively[a]

structure	ΔG^c	$\Delta\Delta G_a^{b,c}$	ΔG^d	$\Delta\Delta G_a^{b,d}$
2	22.3		29.4	
3(ts)	262.5	240.2	278.9	249.5
4	−92.0		−78.2	
4-i	−85.6		−76.0	
3a(ts)	293.2	270.9	307.3	277.9
4a	−43.9		−34.2	
2-w	42.1		58.8	
3-w(ts)	223.2	181.1	243.3	184.5
3a-w(ts)	259.8	217.7	277.4	218.6

[a] Energies are given in kilojoules per mole. [b] $\Delta\Delta G_a$, activation energy. [c] Gibbs free energy from optimized gas phase structure. [d] Single point solvent corrected energy.

Results and Discussion

Nucleophilic Attack at Different Positions. In contrast to carbon dioxide, the nucleophilic attack of hydroxide or water in case of an allene is more complicated. Further, all the problems known from alkenes and alkynes are still present (i.e., the variants of chemo-, regio-, and stereoselectivity aspects). For allenes, there exists a positional selectivity (Figure 1)[47] as the attack can take place at two different positions of the allene molecule. Therefore, additions at one of the orthogonal double bonds will lead to constitutional isomers in the case of substituted allenes, and as a consequence, this inclusion of regioselectivity redoubles the number of isomers. Obviously and supported by our calculations, the attack of the central carbon is preferred as a consequence of charge distribution. The natural population analysis (NPA) yields +0.071 for the central C-atom and −0.511 for the terminal carbons. The oxygen atom in the water molecule has a natural charge of −0.982 and −1.379 in case of hydroxide **5** (see Table 1). However, the attack on the terminal C-atoms is also possible and produces two alcohols **4** and **4a**. The stable 2-propene-1-ol (allyl alcohol) **4a** results from the attack at the terminal carbons, the enol propene-2-ol **4** from the attack at the central carbon. The latter tautomerizes under ambient conditions to give acetone. Compared with **4a**, intermediate **4** results to be the significantly more stable structure ($\Delta\Delta G$ = 48.2 kJ/mol; Scheme 1 and Table 2).

Uncatalyzed Hydration of Allene. "Uncatalyzed reactions" in this context denote water addition reactions without a zinc catalyst but also without any acid or base catalysis. This investigation serves to evaluate the catalytic effect. The reaction paths (i.e., the two nucleophilic attacks of water) are shown in Scheme 1. The first step is the encounter complex **2** of water and allene. It is the same for both reaction paths. The water oxygen lies in opposition to the central C-atom. One water hydrogen is aligned via the π orbital of a double bond. The

(38) Glendening, E. D.; Badenhoop, J. K.; Reed, A. E.; Carpenter, J. E.; Bohmann, J. A.; Morales, C. M.; Weinhold, F. *NBO 5.0*; Board of Regnets of the University of Wisconsin System: Madison, WI, 2001; http://www.chem.wisc.edu/~nbo5/.
(39) Gonzalez, C.; Schlegel, H. B. *J. Chem. Phys.* **1989**, *90*, 2154–2161.
(40) Gonzalez, C.; Schlegel, H. B. *J. Phys. Chem.* **1990**, *94*, 5523–5527.
(41) Helgaker, T.; Uggerud, E.; Jensen, H. J. A. *Chem. Phys. Lett.* **1990**, *173*, 145–150.
(42) Uggerud, E.; Helgaker, T. *J. Am. Chem. Soc.* **1992**, *114*, 4265–4268.
(43) Barone, V.; Cossi, M. *J. Phys. Chem. A* **1998**, *102*, 1995–2001.
(44) Cossi, M.; Rega, N.; Scalmani, G.; Barone, V. *J. Comput. Chem.* **2003**, *24*, 669–681.
(45) Koszinowski, K.; Schroder, D.; Schwarz, H. *Organometallics* **2005**, *24*, 2214–2223.
(46) Schröder, D.; Schwarz, H.; Schenk, S.; Anders, E. *Angew. Chem., Int. Ed.* **2003**, *42*, 5087–5090.
(47) (a) Hashmi, A. S. K. *Angew. Chem.* **2000**, *112*, 3737–3740. (b) Hashmi, A. S. K. *Angew. Chem. Int. Ed. Engl.* **2000**, *39*, 3590–3593.

SCHEME 1. Reaction Path for the Uncatalyzed Hydration of Allene via 4-Membered Cyclic Transition States[a]

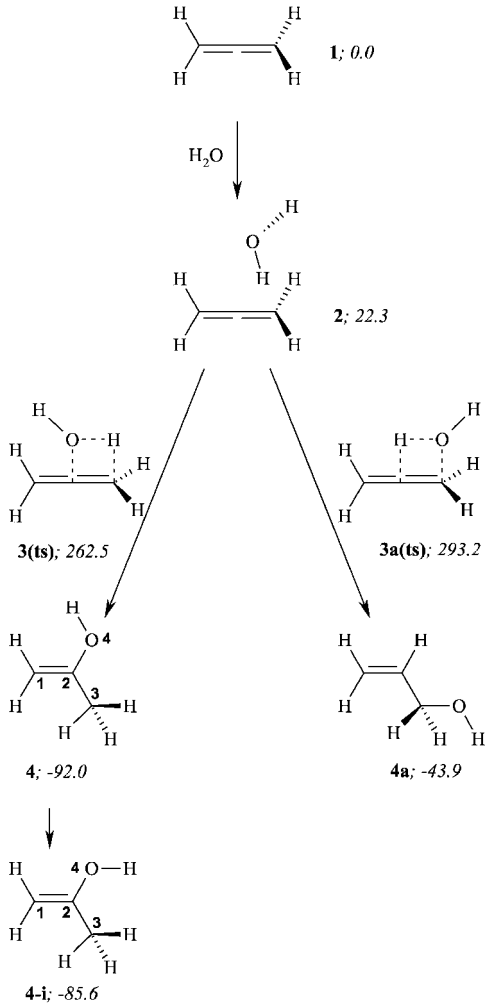

[a] Energies are given in kilojoules per mole.

partial positive hydrogen interacts with the electron-rich π orbital. The oxygen points to the central carbon atom, because the charge analysis indicates a small positive charge at the C(2) atom and negative charges at the terminal C-atoms (see Table 1). The charge of carbon in CO_2 is 1.05 and the corresponding charge of allene carbon is 0.07. Nucleophilic attack on the CO_2 carbon is facilitated but not impossible for allenes. Especially, for the so-called "push−pull" substituted allenes, both nucleophilic and therefore electrophilic reactions are feasible.[48] Allenes as described react with water or alcohols under formation of esters and orthoesters. Although some allene derivatives are known to react instantly under dimerization, stable examples are also found.[49]

Transition states (TS) **3(ts)** and **3a(ts)** (Figure 2) were located, both are 4-membered rings. These strained structures explain the high energy barriers. The Gibbs free energy for **3(ts)** is ΔG = 262.5 kJ/mol which is just $\Delta\Delta G$ = 30.7 kJ/mol lower compared with that of **3a(ts)**. The difference results from the different electrostatic properties in both structures. The arrangement of the atoms involved in the TSs are quite similar. Figure 1 shows the superposition of both TSs. The elongated (partial broken) double bonds are the reference for alignment of both structures. Only small differences in the bond distances, angles, and dihedrals are recognizable. The CCO angle of **3(ts)** is 90.3° and 87.4° for **3a(ts)**. The OHC angles for both structures around the shifted hydrogen differ less than 0.4° (122° in **3(ts)** and 121.6° in **3a(ts)**). This also applies to the bond lengths. The broken CC double bonds have almost the same values (1.386 Å in **3(ts)** and 1.392 Å in **3a(ts)**). Larger varieties exist for the CCC angle. For **3(ts)**, it is 157.4° unlike the angle of 142.1° found in the **3(ts)** structure. These values illustrate the lightweight higher tension in **3a(ts)**. Therefore, uncatalyzed hydration to **4** is preferred kinetically ($\Delta\Delta G$ = 30.7 kJ/mol) and thermodynamically ($\Delta\Delta G$ = 48.1 kJ/mol) in contrast to **4a** (cf. Table 2). However, the barriers are so high that a reaction is impossible under normal conditions. A reaction may become possible under somewhat extreme conditions involving increased pressure and temperature, but oligomerization of allene as competitive reaction can also pass off. Acid or base catalysis is the more reliable way, but it is restricted comparable to the zinc catalyzed reaction paths due to the ionic procedure.

Scheme 1 shows an additional structure **4-i** after the uncatalyzed reaction to product **4**. Both structures are potential products for the catalyzed reaction pathways as well and hence are described here. **4-i** differs from **4** with regard to the orientation of the hydroxide group. **4** is ($\Delta\Delta G$ = 6.5 kJ/mol) more stable, although the shortest HH distance (between hydroxide and methylene group) is only 2.299 Å (d = 2.436 Å for **4-i** between the hydroxide and methyl group). The steric strain at the terminal C hydrogens is not relevant, because it is similar for both structures (distance 2.438 Å in **4** and 2.426 Å in **4-i**, respectively).

This difference can be explained by negative hyperconjugation.[50] This effect results in an interaction of a heteroatom lone pair with an acceptor σ^* orbital. Despite the fact that originally sp^3 configurated carbons were investigated, such effects can be observed for carbons with sp^2 hybridization, too. Energy $E(2)$, a second-order perturbation approach estimating the interaction energy between the orbitals, is used for quantification.[51]

Water Catalyzed Hydration of Allene. Another focus was the determination of the water catalyzed hydration (Scheme 2). This reaction proceeds with two water molecules via an enlarged 6-membered cyclic TS instead of a 4-membered ring (Schemes 1 and 2). **4** and, respectively, **4a** are formed, and a water molecule is regenerated. For differentiation, such structures and TSs are indicated by the additional letter "**w**". In relation to geometry, **2-w** is comparable to **2** with additive water. This second water forms a hydrogen bond to the other oxygen (d = 1.907 Å). Accordingly, the reaction path leads to the transition states **3-w(ts)** or **3a-w(ts)** (Figure 2). Relaxation results in a

(48) Saalfrank, R. W. *Tetrahedron Lett.* **1973**, *14*, 3985–3988.
(49) Saalfrank, R. W. *Tetrahedron Lett.* **1975**, *16*, 4405–4408.

(50) Nilsson Lill, S. O.; Rauhut, G.; Anders, E. *Chem.—Eur. J.* **2003**, *9*, 3143–3153.

(51) Equation $E(2) = -n_{lp}F_{ij}^2/\Delta\varepsilon$ describes the $E(2)$ estimation, n_{lp} is the occupancy number of the lone pair, F_{ij} the Fock matrix element between orbitals i and j, and $\Delta\varepsilon$ is the energy gap between the two interacting orbitals. $E(2)$ for the interaction of the first lone pair of oxygen with σ^* orbital of the CC double bond in **4** amounts to 30.5 kJ/mol. In **4-i**, this lone pair must interact with the σ^* orbital of the CC single bond ($E(2)$ = 28.0 kJ/mol). Next to this "classical" negative hyperconjugation, further interactions exist between the second lone pair of the oxygen and the π^* orbital of the CC double bond in both isomers. The second lone pair has 99.8% π character. For this interaction, $E(2)$ amounts to 152.7 kJ/mol in **4-i** and 160.6 kJ/mol in **4**. All these interactions lead to bond contractions and bond elongations, respectively, depending on the nature of the bonds to which the antibonding orbitals are belonging. Hence, the CC double bond distance is 1.332 Å in **4** and 1.329 Å in **4-i**. Conversely, the CC single bond distance is 1.486 Å in **4** and 1.489 Å in **4-i**. Furthermore, the 0.004 Å longer CO distance in **4-i** shows that the negative hyperconjugation in this structure is expressed to a lesser extent.

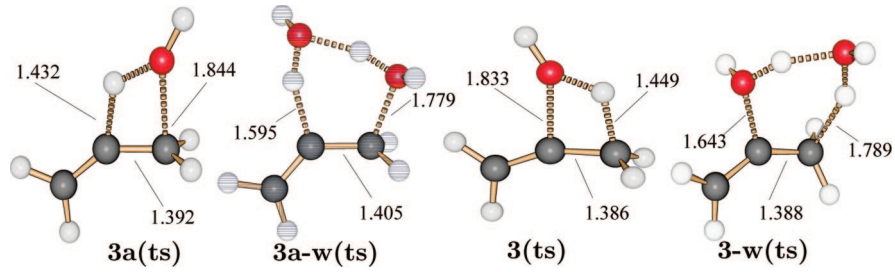

FIGURE 2. Calculated transition structures for **3(ts)** and **3a(ts)**. The TSs **3a-w(ts)** and **3-w(ts)** contain an additional molecule of water, the "catalyst". Distances are given in angstroms. The colors are as follows: red, oxygen; black, carbon; and white, hydrogen.

SCHEME 2. Uncatalyzed Reaction of Allene with Two Water Molecules via 6-Membered Cyclic Transition States[a]

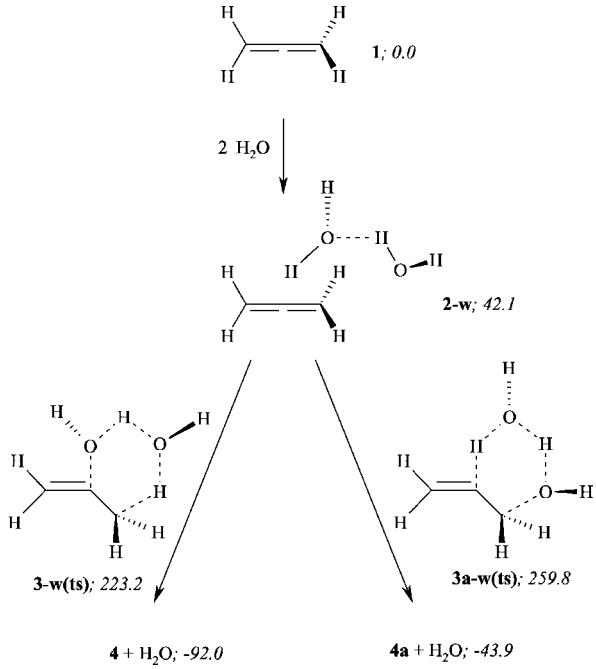

[a] Energies are given in kilojoules per mole.

lower activation barrier for the formation **3-w(ts)** in comparison to **3(ts)** ($\Delta\Delta G$ = 39.3 kJ/mol; see Table 2). Activation barriers differ by $\Delta\Delta G$ = 59.1 kJ/mol relative to the preceding water encounter complexes **2** and **2-w** because of the $\Delta\Delta G$ = 19.8 kJ/mol difference between both of them. ΔG = 223.2 kJ/mol is still a rather high energy barrier. A slightly lower catalytic effect can be observed between **3a-w(ts)** and **3a(ts)** ($\Delta\Delta G$ = 33.4 kJ/mol and $\Delta\Delta G$ = 53.2 kJ/mol in relation to **2** and **2-w**). The energy value is ΔG = 259.8 kJ/mol) for **3a-w(ts)** (see Table 2).

Catalytic Cycle for the $[(NH_3)_3ZnOH]^+$-Mediated Hydration of Allene. The first step of searching for the reaction path is comparable with the procedure applied for the uncatalyzed reaction. Hydroxide has an affinity to the central and terminal carbon atoms. To check whether the nucleophilic attack on the central carbon is energetically favorable, we performed DFT calculations in order to get the relative activation barriers. The resulting pathway and structures involved are shown in Scheme 3. At the beginning, the model complex $[(NH_3)_3ZnOH]^+$ and the allene molecule form an encounter complex **6** from which both reaction paths start. This structure has C_s-symmetry with the carbon backbone, hydroxide, the metal ion, and one ammonia ligand in the symmetry plane. Allene is located opposite to the hydroxide group, similar to **2**. The distance between hydroxidic hydrogen and the central allenic carbon atom amounts to 2.516 Å, and the nearest terminal carbon is at 2.693 Å. **6** is destabilized (ΔG = 29.3 kJ/mol) in comparison to the separated reactants **5** and allene.

Reaction Path for Nucleophilic Attack at the Terminal Carbon Atom of Allene (Schemes 3 and 4 and Figure 3). Continuing from the encounter complex **6**, the transition state **7a(ts)** has to be surmounted. This structure is a trigonal bipyramid with a hydroxide group and two ammonia ligands as equatorial plane and the third ammonia and central carbon atom as axis. The off-axis angle CZnN amounts to 10.8°. The hydroxidic oxygen, central zinc atom, and the two carbon atoms form a 4-membered cyclic transition state. The π-CC bond and ZnO bond are broken simultaneously; new ZnC and CO bonds are formed. The distance between Zn and the central C atom results in 2.284 Å. The Gibbs free energy value is ΔG = 139.3 kJ/mol in relation to the free educts and $\Delta\Delta G$ = 109.9 kJ/mol in relation to **6**.

7a(ts) relaxes to give the intermediate **8a** (Figure 3). This structure has C_s-symmetry comparable to that of **6**. The carbon backbone, hydroxide, the metal ion, and one ammonia ligand span the symmetry plane. The now carbon bound oxygen forms two hydrogen bonds (d = 2.318 Å) to the adjacent ammonia ligands. Thus, the hydroxide is placed between and in front of the ligands. The ZnC distance is now 1.959 Å. $\Delta\Delta G$ between **7a(ts)** and **8a** is 159.4 kJ/mol. Therefore, the intermediate is $\Delta\Delta G$ = 20.2 kJ/mol more stable than the separated reactants.

The insertion of a water molecule into the reaction system is the consecutive step (Scheme 4). It approximates perpendicularly to the symmetry plane so that two positions of attack are possible. Both are mirror-symmetric so that only one way is described and displayed. Water is stabilized by two hydrogen bonds to the ligands. This results in a small stabilization of $\Delta\Delta G$ = 2.7 kJ/mol (**9a**; see Figure 4). One water hydrogen is located 2.508 Å in front of the central carbon. The distance between the water oxygen and zinc is 3.114 Å. The appropriate ammonia ligand is about 4° out of the symmetry plane due to the hydrogen bonds.

Continuation of the reaction path results in the 4-membered cyclic transition state **10a(ts)**. It is far away to be a perfect quadrangle. The geometric form of the participating atoms resembles a triangle with zinc, carbon, and oxygen as corners. With 163.5°, the CHO angle is near the theoretical value of 180°. This is the reason why hydrogen is only 1.939 Å remote from the zinc, whereas the distance between zinc and the water oxygen is 2.118 Å. **10a(ts)** has a ΔG = 81.9 kJ/mol relative to free allene and **5** and an activation barrier of $\Delta\Delta G_a$ = 104.8 kJ/mol relative to the water encounter complex **9a**. **11a** is the product complex after **10a(ts)** and consists of the initial zinc hydroxide complex **5** and allyl alcohol **4a**. $\Delta\Delta G$ from **10a(ts)**

SCHEME 3. First Part of the Catalyzed Reaction: Reaction Paths for the Nucleophilic Attack at the Central or the Terminal Carbon Atoms of the Reaction between $[(NH_3)_3ZnOH]^+$ (5) and allene (1)[a]

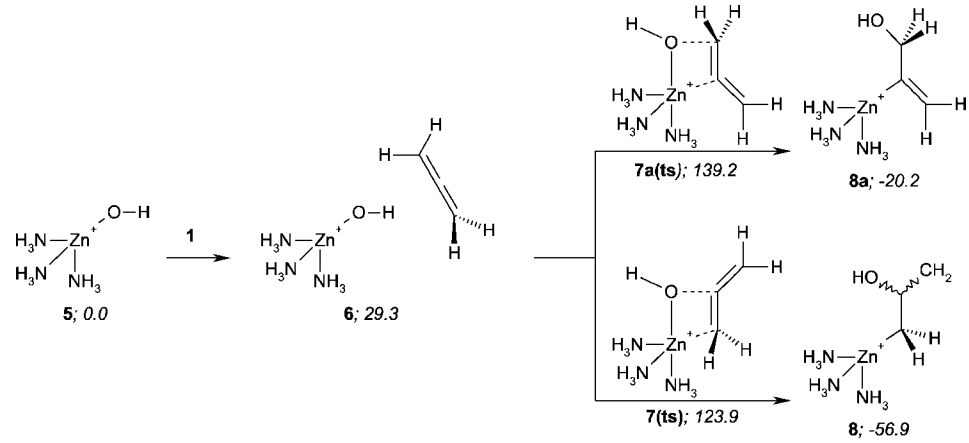

[a] Energies are given in kilojoules per mole.

SCHEME 4. Second Part of the Catalyzed Reaction to 4a: Addition of an External Water Molecule (Formation of 11a), Regeneration of the Catalyst 5, and Formation of the Product 4a[a]

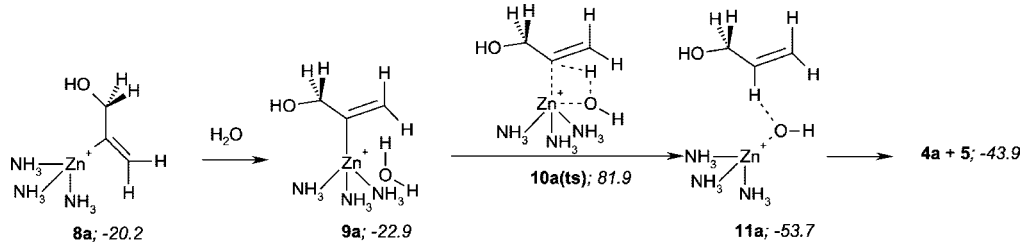

[a] Energies are given in kilojoules per mole.

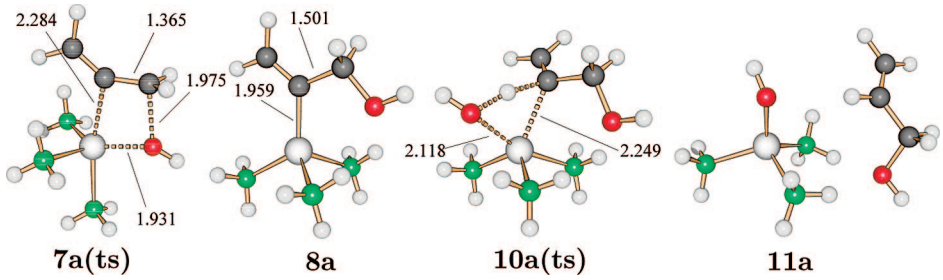

FIGURE 3. Calculated structures of selected stationary points along the reaction coordinate of the reaction between $[(NH_3)_3ZnOH]^+$ (**5**) and allene (**1**) to allyl alcohol (**4a**). Distances are given in angstroms. The colors are as follows: red, oxygen; green, nitrogen; black, carbon; white, hydrogen; and gray, zinc.

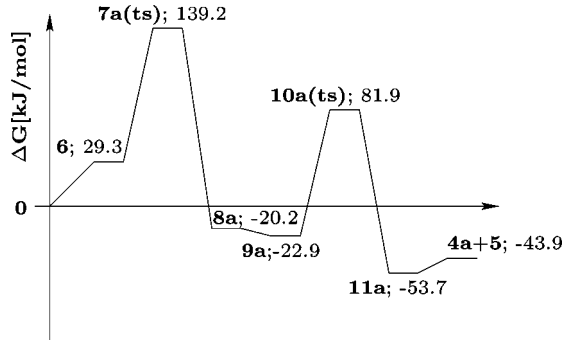

FIGURE 4. Gibbs free energy as a function of the reaction coordinate of the reaction between $[(NH_3)_3ZnOH]^+$ (**5**), allene (**1**), and water (formation of allyl alcohol **4a**).

to **11a** is −135.6 kJ/mol; **11a** is by $\Delta\Delta G = 9.8$ kJ/mol more stable in comparison to the separated products **4a** and **5**. The stabilization results from the two hydrogen bonds between the alcohol oxygen and hydrogens from two ammonia ligands. Furthermore, there exists an interaction between the oxygen of **5** and the hydrogen at the central carbon of **4a**.

Reaction Path for Nucleophilic Attack at the Central Carbon Atom of Allene (Scheme 3). The second variant of the nucleophilic attack is that at the central carbon atom of the allene molecule. Similar to the nucleophilic attack at the terminal carbon atom of allene, this path starts with structure **6** (Scheme 3 and Figure 7). The transition state **7(ts)** is the rate-determining step and also the structural analog for the rate-determining step in the CO_2 or COS reaction paths.[52]

7(ts) (Figure 7) has a quadratic pyramidal structure with allene carbon and the aggressing oxygen in plane and one ligand nitrogen as the vertex. The attacked double bond is elongated (1.363 Å). Oxygen is 1.941 Å separated from zinc and 2.047 Å approximated to the central carbon. The CZnO angle of 79.7° reduces the strain of the 4-membered ring so that the CCO angle of these at the TS participating atoms is 103.5°. Compared with

SCHEME 5. Predominant Mesomeric Structures of the Intermediate 8

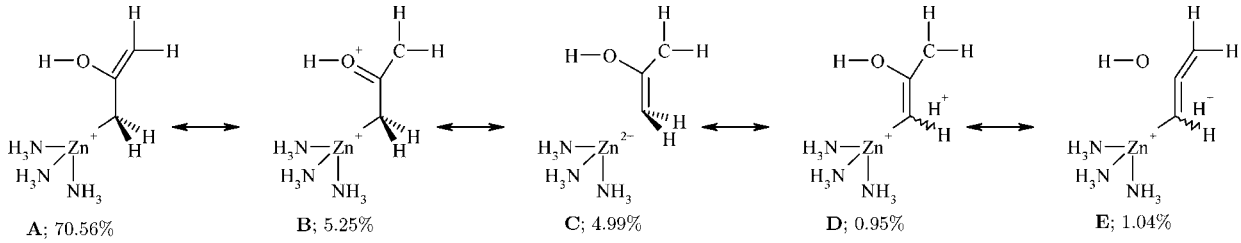

SCHEME 6. Schematic Depiction of the Lindskog Equivalent Mechanism of the Rotation around the CC Bonding Axis of the Zn Bound Carbon and the Central Carbon Atom[a]

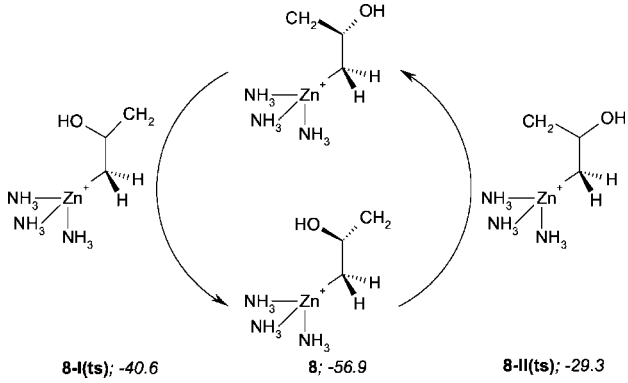

[a] Energies are given in kilojoules per mole.

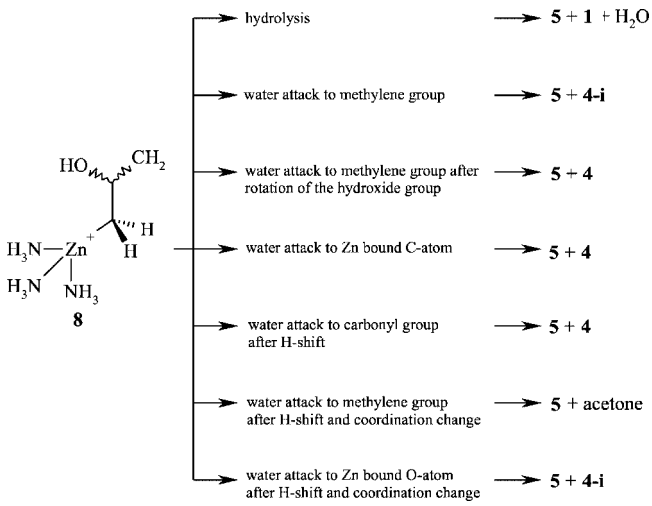

FIGURE 5. Overview of possible reaction paths starting from the key intermediate **8** and the resulting products.

the water catalyzed reaction, the activation barrier for the zinc-mediated attack is significantly reduced by more, roughly 100 kJ/mol (from 223.2 to 123.9 kJ/mol, Schemes 2 and 3). As with the other 4-membered ring transition states, the formation of **8** via **7(ts)** is a concerted reaction (Scheme 5). The activation barrier for the nucleophilic attack of the zinc hydroxide complex on the allene is more than twice as high as for the reaction with CO_2 ($\Delta G = 55.6$ kJ/mol calculated at the mPW1k/aug-cc-pVDZ level) and after all only a third higher as for the reaction with COS ($\Delta G = 84.2$ kJ/mol for the sulfur attack on zinc; $\Delta G = 95.9$ kJ/mol for the oxygen attack on zinc; each at the B3LYP/6-311+G(d,p) level).[52]

At this point, a comparison of the allene, carbon dioxide, and the important and reactive "in between" heteroallen ketene is useful. All natural charges are shown in Table 1. For allene, a strong displacement of electron density is necessary in the transition state **7(ts)** (see below). The charge of the reacting terminal carbon changes to −0.912 ($\Delta = 0.4$). For CO_2, the difference of the charge of the correspondent oxygen is only $\Delta = 0.22$ and negligible $\Delta = 0.009$ for the central carbon. In the case of ketene, two variants of the nucleophilic attack exist. In the CO_2 equivalent case, the change of the central carbon natural charge is very small ($\Delta = 0.033$) in the transition state. In the allene equivalent second case, the charge of the central carbon changes $\Delta = 0.144$ and $\Delta = 0.3$ for the terminal carbon. The activation barrier for the CO attack on ketene ($\Delta G = 36.6$ kJ/mol) is on the half-level of the CC attack ($\Delta G = 75.9$ kJ/mol). That implies that a stronger displacement of electron density correlates to a lower activation barrier.

As depicted in Scheme 6 and Figure 5, the compound **8** plays the role of an interesting key intermediate in the catalyzed reaction.

8 exists in two isomeric forms. A clockwise and counterclockwise rotation around the single bond between the zinc bound carbon and the central carbon atom can interconvert the two isomers. As a result, the two C_s-symmetric transition states **8-I(ts)** and **8-II(ts)** were found. The symmetry plane goes through all atoms except two ammonia ligands, two hydrogens from the third ammonia, and the two hydrogens at the zinc bound carbon. At **8-I(ts)**, the hydroxide group points to the ammonia ligand. In **8-II(ts)**, the hydroxide and methylene groups are interchanged. **8-I(ts)** is stabilized due to hydrogen bond interactions in contrast to **8-II(ts)**. The activation barriers for the conversion of both isomers **8** into one another amount to $\Delta\Delta G_a = 16.3$ kJ/mol (**8-I(ts)**) and $\Delta\Delta G_a = 27.6$ kJ/mol (**8-II(ts)**).

In comparison, the proposed analog transition state for catalytic cycle for the CO_2 hydration[18] and the transition state **7(ts)** result to be quite similar. In contrast to **8**, the following so-called Lindskog-type intermediate[53] is C_s-symmetric like **8-I(ts)**. The geometric structure of intermediate **8** is comparable to the Lindskog-type rotational TS which leads to the Lipscomb product. The latter is a geometrical equivalent to **8-II(ts)**. An alternative way, like Lipscomb mechanism (proton shift)[54,55] appears to be impossible for intermediate **8** due to the different geometry. At first inspection, there is no reason for special geometrical properties of **8**. NRT (natural resonance theory) calculations[56−58] and Wiberg bond indices[59] give an explanation. This index for the ZnC bond is 0.36 and 1.11 for the CC single bond. The NRT calculation explains the partial double bond character for this CC single bond.

Scheme 5 shows the most important mesomeric structures. Stucture **A** has the highest resonance weight of 70.56% and represents **8** in all reaction schemes. Structure **B** has a negative partial charge on the remote methylene group and a double bond with positive partial charge on oxygen. **C** is

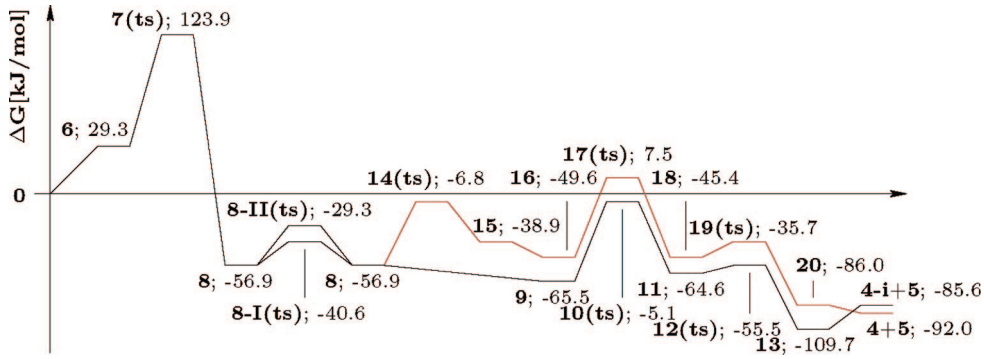

FIGURE 6. Energy profiles for the reaction of $[(NH_3)_3ZnOH]^+$ (**5**) and allene (**1**) to propen-2-ol (**4** and **4-i**) with water attack on the methylene group with and without a preceding rotation of the hydroxide group. The lowest energy barrier of metal free hydration of allene is $\Delta G = 223.2$ kJ/mol (structure **3-w(ts)**, cf. Table 2).

SCHEME 7. Reaction Paths for Water Attack to 8 Followed by a Hydrogen Shift to the Methylene Group via a 6-Membered Cyclic Transition State with and without Rotation of the Hydroxide Group[a]

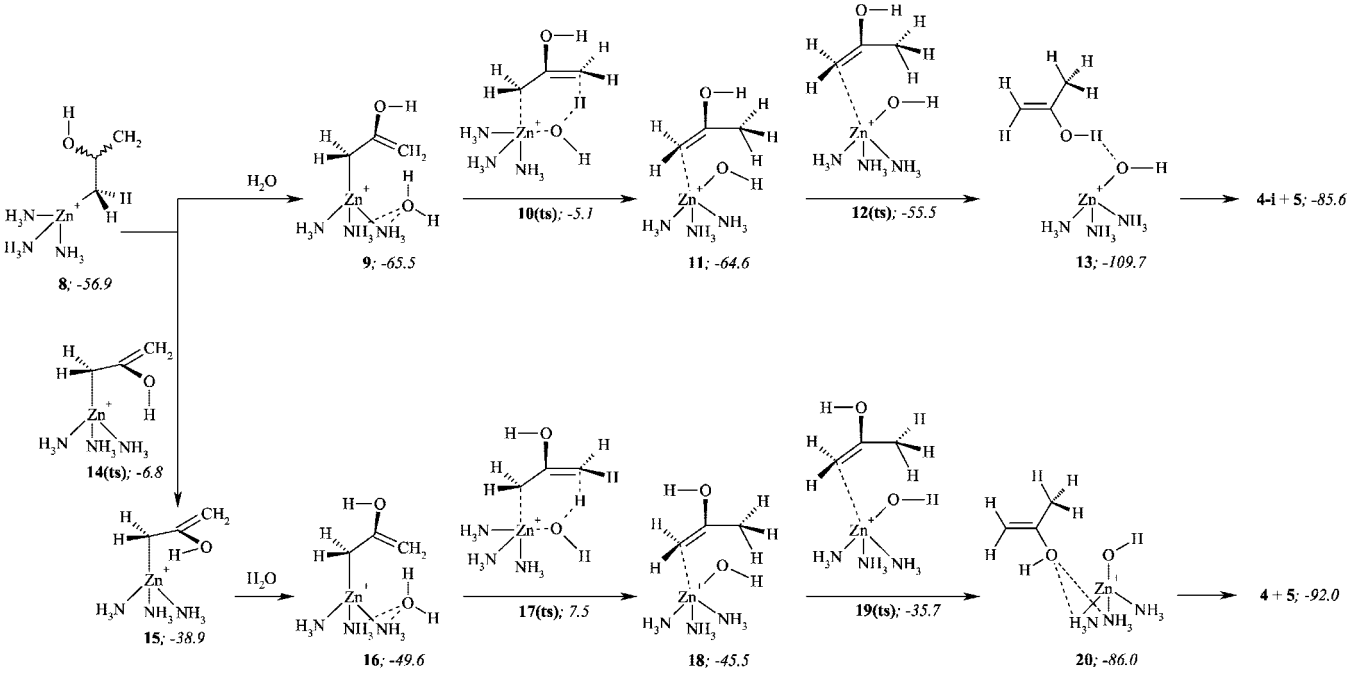

[a] Energies are given in kilojoules per mole.

the best mesomeric structure to explain the special geometry of **8**. **C** has a double bond between the Zn bound and the central carbon atoms. Therefore, the hydroxide and the methylene group are not able to stand perpendicular to the plane spanned by the ammonia ligands. The carbon backbone and the oxygen roughly form a parallel plane to it. **B** and **C** have resonance weights of 5.25% and 4.99%. **D** and **E** form another mesomeric structure with double bonds between Zn bound and the central carbon atoms, but have only resonance weights of about 1% each.

Many reaction paths were found starting with the key intermediate **8** (Scheme 5). Hydrolysis recreates allene and the zinc complex. One way leads to acetone. For all other paths, the catalytic products are **4** or the isomer **4-i**. ΔG relative to the free educts is −144.7 kJ/mol for acetone, 92.0 kJ/mol for **4**, and 85.6 kJ/mol for **4-i** (cf. Figures 6 and 8).

Reaction Paths Starting from Key Intermediate 8. The introduction of one water molecule can take place at different positions (Scheme 7). Stable water encounter complexes result from hydrogen bonds between ammonia hydrogen and water oxygen. **9** is stabilized further by an interaction of the π orbital of CC double bond with the σ^* orbital of the water HO bond ($E(2) = 52.9$ kJ/mol). The distance between the water hydrogen and the terminal carbon of the double bond is 2.109 Å. Therefore, **9** is $\Delta\Delta G = 8.6$ kJ/mol more stable in comparison to **8** and the free water molecule (Scheme 7). The water oxygen is located 3.295 Å away from the central Zn atom. Both CC bonds are of quite the same lengths (1.408/1.486 Å, Wiberg bond indices 1.309/1.381; see Figure 7). The energy barrier from

(52) Schenk, S.; Kesselmeier, J.; Anders, E. *Chem.—Eur. J.* **2004**, *10*, 3091–3105.

(53) Lindskog, S.; Henderson, L.; Kannan, K. K.; Liljas, A.; Nyman, P. O.; Strandberg, B. *The Enzymes*, 3rd ed.; Accademic Press: New York, 1971; Vol. 5, p 587.

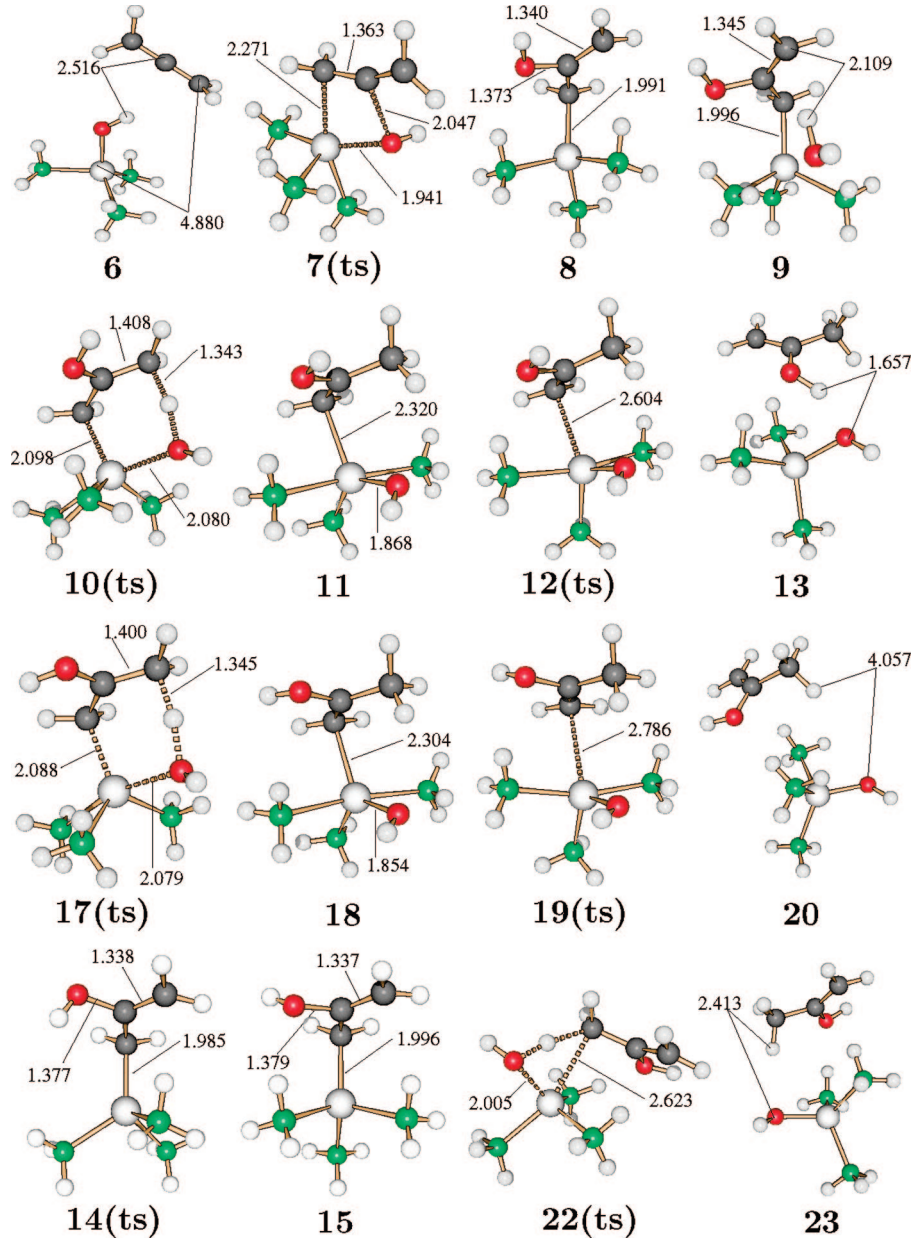

FIGURE 7. Calculated structures of selected stationary points for the reaction of $[(NH_3)_3ZnOH]^+$ (**5**) and allene (**1**) to propen-2-ol (**4** and **4-i**) with water attack on the methylene group with and without a preceding rotation of the hydroxide group. Distances are given in angstroms. The colors are as follows: red, oxygen; green, nitrogen; black, carbon; white, hydrogen; and gray, zinc.

9 to **11** amounts to $\Delta\Delta G_a = 60.4$ kJ/mol. The proton is shifted in a 6-membered cyclic transition state **10(ts)** to the intermediate **11** and not directly to the product encounter complex **13**. **11** has a trigonal bipyramidic geometry with two ammonia ligands as axis. The ZnC bond is not completely broken ($d = 2.320$ Å). The ZnO bond distance is 1.868 Å ($d = 1.825$ Å in **5**). The energy $E(2)$ between the CC double bond π orbital and the antibonding lone pair (99.7% s-character) from Zn amounts to 158.7 kJ/mol (for comparison, between same antibonding lone pair of Zn and the lone pair of the equatorial ammonia nitrogen $E(2) = 185.4$ kJ/mol). To obtain the product encounter complex **13**, the energy barrier of the transition state **12(ts)** must surmounted ($\Delta\Delta G = 9.1$ kJ/mol). It is "the countermovement" to take up **4-i** by **5**. The shortest ZnC bond length is 2.604 Å to the external sp^2 hybridized carbon. The energy gain for **13** is $\Delta\Delta G = -54.2$ kJ/mol, but $\Delta\Delta G = 24.1$ kJ/mol to obtain the free molecules **4-i** and **5**.

The transition state **10(ts)** is the equivalent TS of the water addition to the intermediate in the CO_2 reaction path.[52] With CO_2 as substrate, the water attack is almost barrier-free.

If the hydroxide group rotates 180° around the CO bond before water attacks to **8**, the more stable product **4** is obtained. **14(ts)** represents the rotational TS. The hydroxide is orthogonal to the plane spanned by the carbon backbone. The energy barrier for rotation is $\Delta\Delta G_a = 51.1$ kJ/mol, and the energy of the intermediate **15** is $\Delta G = 38.9$ kJ/mol. The energetical difference between **8** and **15** stems from the same negative hyperconjugative effect as between **4** and **4-i**. The interaction of the second oxygen lone pair (92.65% p-character) and the π^* orbital of the CC double bond amounts to $E(2) = 134.9$ kJ/mol for **8** and

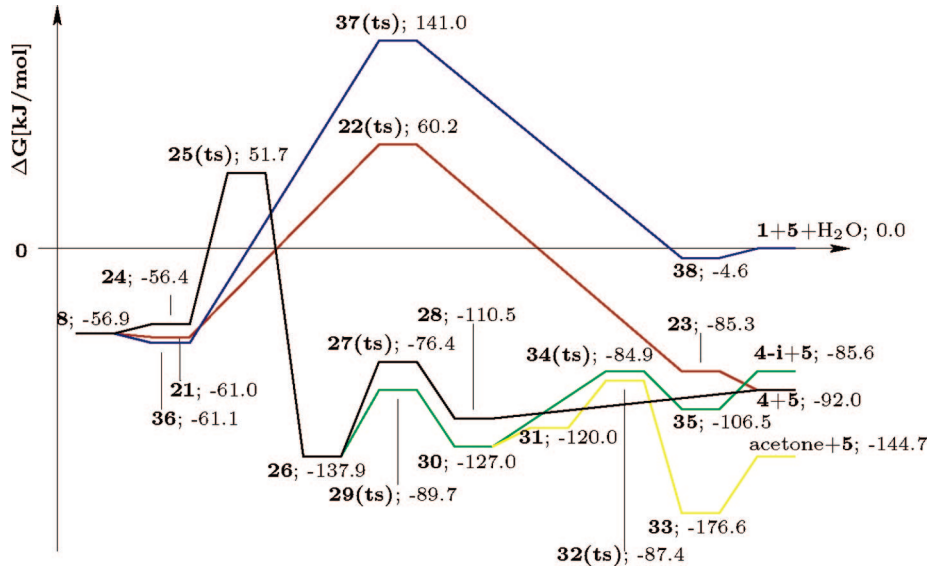

FIGURE 8. Water catalyzed H-shift over a 6-membered cyclic transition state starting with intermediate **8** and pursuing reaction paths as shown in Schemes 9 and 10.

SCHEME 8. Reaction Path for Water Attack on the Zn Bound C Atom over a 4-Membered Cyclic Transition State Starting with Intermediate 8[a]

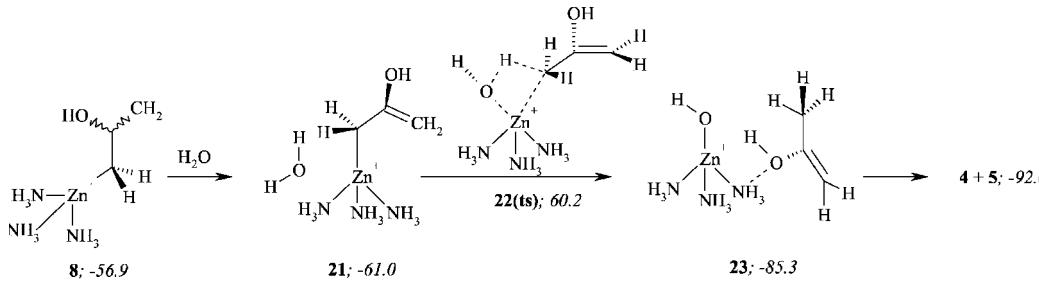

[a] Relative energies are given in kilojoules per mole.

only $E(2) = 74.1$ kJ/mol for **15**. The negative hyperconjugation between the first lone pair of oxygen with the σ^* orbital of the CC double bond in **8** amounts to $E(2) = 27.2$ kJ/mol. For **15**, this lone pair must interact with the σ^* orbital of the CC single bond ($E(2) = 29.4$ kJ/mol).

Continuation of the reaction path (structures **16** to **20**) results in a similar description compared to the structures **9**−**13** (Scheme 7 and Figure 7). There are no differences in the mechanism for both reaction paths. The progress of the Gibbs free energy for the OH group rotated path is about $\Delta\Delta G =$ 16−20 kJ/mol parallel above to the unrotated variant due to the same reasons as described for **8** and **15**. Only the product complexes **13** and **20** show a slightly lager difference ($\Delta\Delta G =$ 23.7 kJ/mol). The product **4-i** results from **13** (endergonic step; $\Delta\Delta G = 24.1$ kJ/mol), whereas **20** gives the more stable isomer **4** (Figure 6; exergonic step; $\Delta\Delta G = -6.0$ kJ/mol). Both reaction paths are the most probable variants as remains to be seen (vide infra). All others have higher barriers to close the catalytic cycle.

Starting with the key intermediate **8**, further stable water encounter complexes were calculated. The water molecule can be positioned in the two other gaps between the ammonia ligands (structure **21**; Scheme 8). As in **9** or **16**, hydrogen bonds between oxygen and one of each of the ammonia hydrogens stabilizes **21**. In contrast to **9** or **16**, it lacks the attraction to the methylene group π system. Therefore, the distance between the water hydrogen and the zinc bound carbon is 4.655 Å in contrast to the 2.109 Å in **9**. The distance between Zn and the water oxygen is 3.844 Å. **21** has $\Delta G = -61.0$ kJ/mol and is only $\Delta\Delta G = -4.1$ kJ/mol more stable than **8**. The water encounter complex **21** exists in two mirror-symmetric variants with the water molecule on one side of the symmetry plane spanned by the opposite ammonia nitrogen, zinc, and the zinc bound carbon.

The transition state **22(ts)** follows, its geometry is similar to that of **10a(ts)** (Figure 3)—a 4-membered ring assembly. Hydrogen from water is shifted to the zinc bound carbon atom, and simultaneously, the water oxygen attacks the zinc ion. The CHO angle is 167.9°, and the shifted hydrogen is only 2.014 Å afar from zinc (ZnO distance $d = 2.005$ Å). The zinc bound carbon is already 2.623 Å remote from zinc. Altogether, it is a significantly strained TS though this strain is slightly reduced by a hydrogen bond between an ammonia hydrogen and the hydroxidic oxygen ($d = 1.898$ Å) as well as by an interaction of a further ammonia hydrogen with the methylene group π system ($d = 2.194$ Å). The energy barrier from **21** is $\Delta\Delta G_a =$ 121.2 kJ/mol and $\Delta G = 60.2$ kJ/mol relative to free educts. Accordingly the activation barrier is quite as high as for the initial allene attack to the zinc complex. Therefore this variant is more improbable. **22(ts)** relaxes to give the product complex **23**. The interactions between the hydrogens of the ammonia ligands and the methylen group π system ($d = 2.382$ Å) as well as the hydrogen bond ($d = 2.005$ Å) still exist. The energy of **23** is $\Delta G = -85.3$ kJ/mol and $\Delta G = -92.0$ kJ/mol for the free products **5** and **4**.

SCHEME 9. Reaction Paths for the Water Catalyzed H-Shift via a 6-Membered Cyclic Transition State 25 Starting from the Key Intermediate 8 and Further Steps[a]

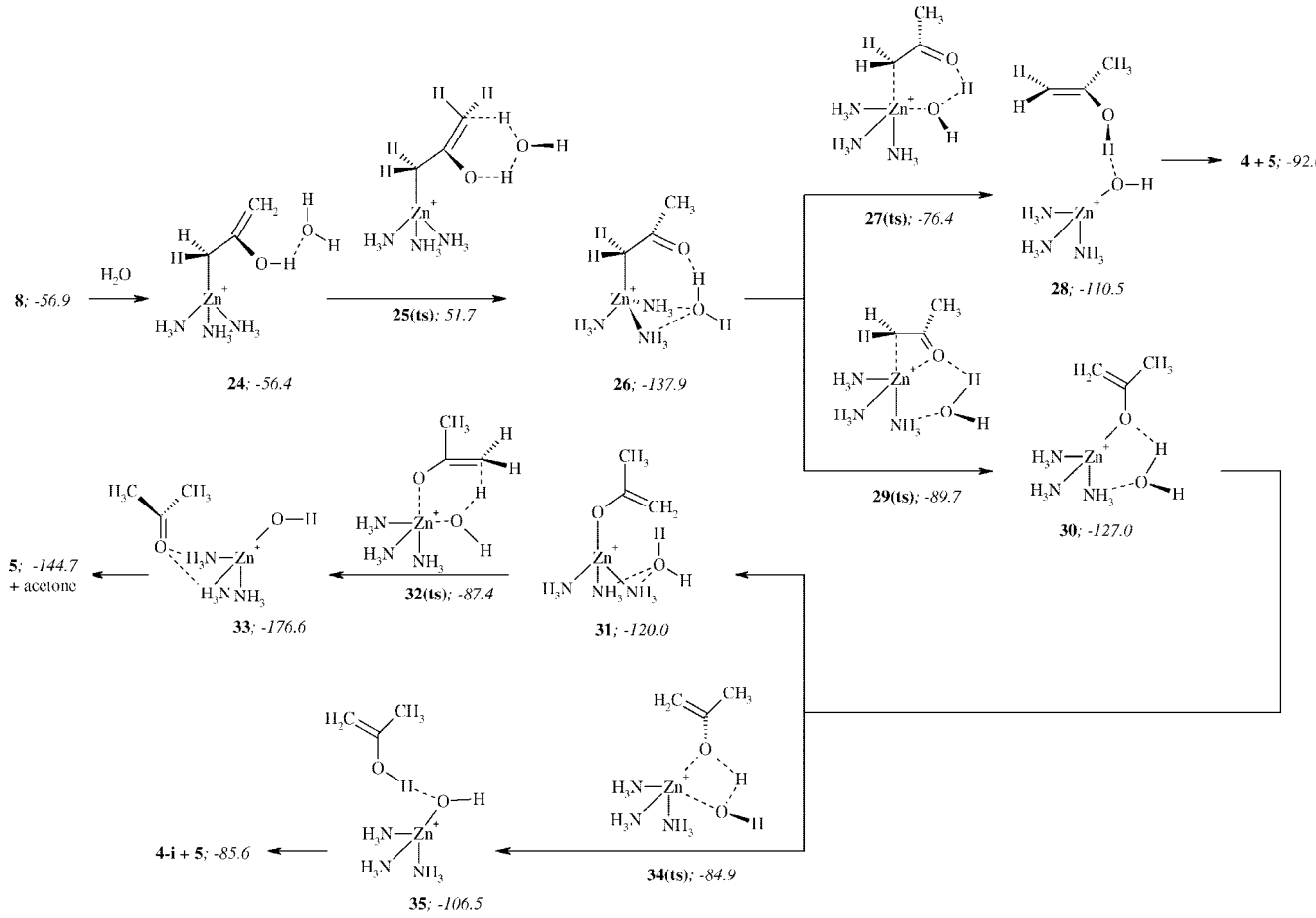

[a] Relative energies are given in kilojoules per mole.

SCHEME 10. Decomposition of the Key Intermediate 8 under Formation of the Educts via a 6-Membered Cyclic Transition State, 37(ts)[a]

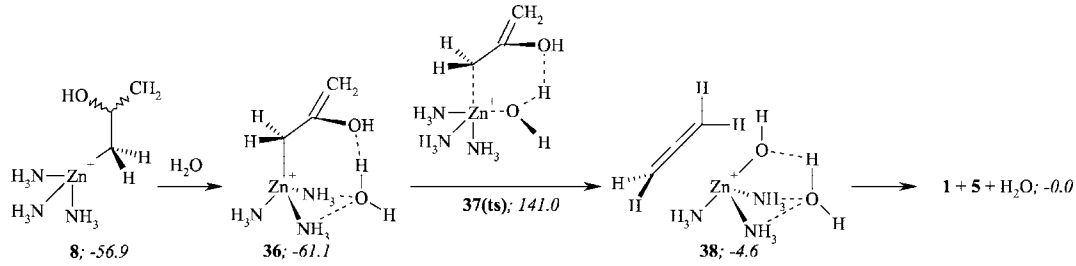

[a] Relative energies are given in kilojoules per mole.

A proton shift, equivalent to the Lindskog mechanism[54,55] is impossible in the case of intermediate **8** for the reasons described above. Nevertheless, a proton shift from hydroxide to the methylene group is possible. The water catalyzed variant via a 6-membered cyclic TS is described here (Scheme 9). In the water encounter complex **24** exists a hydrogen bond between the hydroxidic hydrogen and the water oxygen (d = 1.778 Å). The distance between the ensuing shifted water hydrogen and the terminal carbon is 3.507 Å. The bond length of the CC double bond is 1.344 Å. The energy of **24** is quite the same as for **8**.

In the next step, the 6-membered cyclic TS **25(ts)** is formed. The corresponding activation barrier is $\Delta\Delta G$ = 108.1 kJ/mol. This barrier is lower than for **22(ts)** but obviously higher than for **10(ts)** or **17(ts)** (Scheme 7). The to be shifted hydrogen is 1.512 Å remote from the terminal carbon. The CC double bond is elongated to 1.408 Å. **25(ts)** relaxes to give the intermediate **26**, which has a carbonyl and methyl group instead of a hydroxide and methylene group. A new molecule of water is formed, which moves barrier-free to the ligand sphere. There exist hydrogen bonds between an ammonia hydrogen and the water oxygen as well as between the water hydrogen and the carbonyl oxygen. **26** is $\Delta\Delta G$ = −81.5 kJ/mol more stable than the water encounter complex **24**. With an energy value of ΔG = −137.9 kJ/mol relative to the free educts, this complex **26** is the most stable intermediate found so far.

A proton transfer to the carbonyl group is perfectly preconfigured in **26**. $\Delta\Delta G$ = 61.5 kJ/mol are needed to reach the

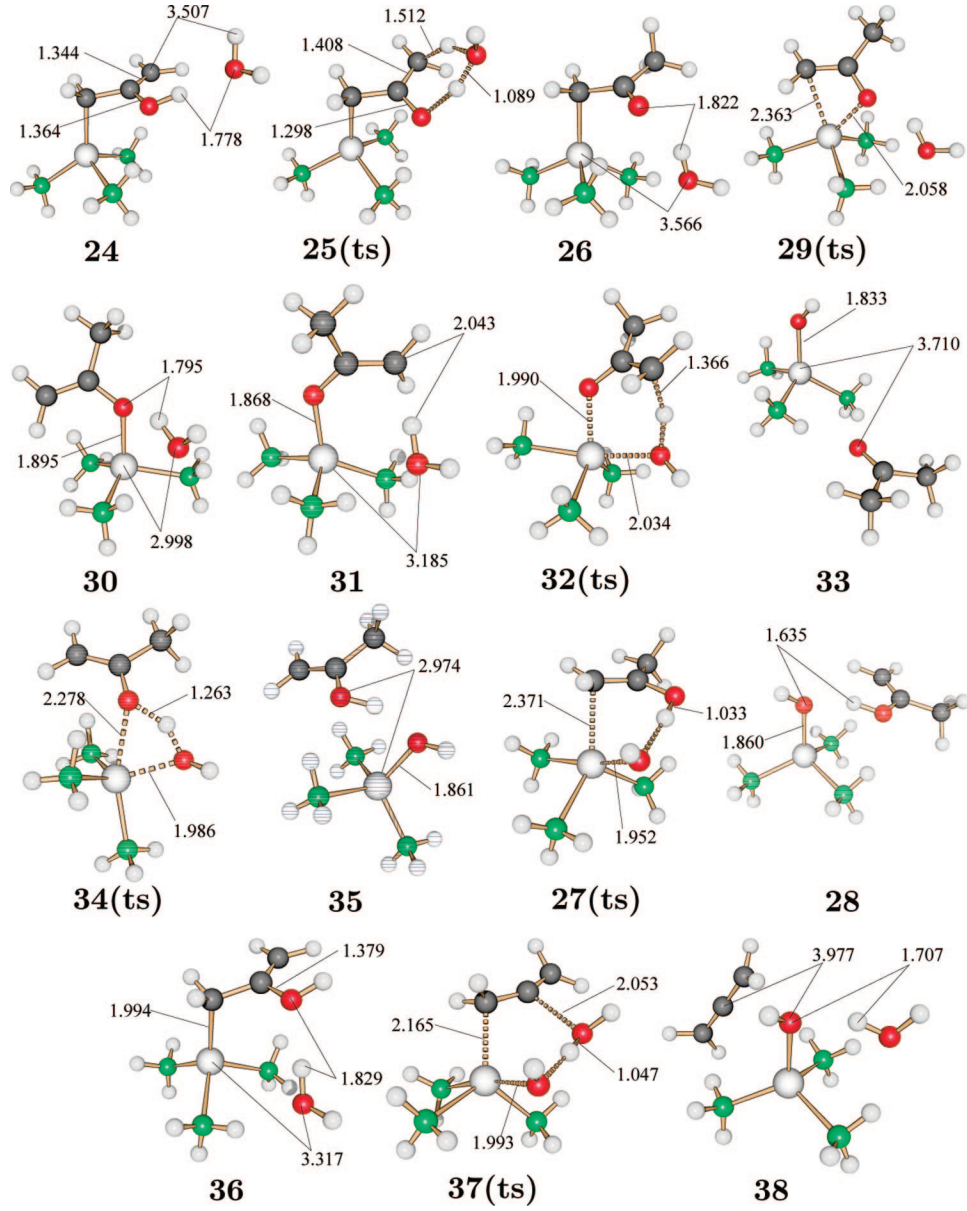

FIGURE 9. Calculated structures of selected stationary points of the reaction coordinate for the water catalyzed H-shift via a 6-membered cyclic transition state, starting with the key intermediate **8** (Schemes 9 and 10). Distances are given in angstroms. The colors are as follows: red, oxygen; green, nitrogen; black, carbon; white, hydrogen; and gray, zinc.

6-membered cyclic TS **27(ts)**, in which the distance between the zinc and water oxygen is reduced to 1.952 Å. The shifted hydrogen is already located 1.033 Å near to the carbonyl oxygen. **27(ts)** relaxes to give structure **28**, which consists of product **4** and the initial zinc hydroxide complex **5**. **28** is stabilized in due to a hydrogen bond (d = 1.635 Å). But, the Gibbs free energy is only $\Delta G = -110.5$ kJ/mol for **28** and as a consequence only $\Delta\Delta G = -34.1$ kJ/mol lower relative to **27(ts)**. This part of the reaction path is endergonic ($\Delta\Delta G$ = 27.4 kJ/mol). Additionally, $\Delta\Delta G$ = 18.5 kJ/mol must be provided to get the free products **4** and **5** (Figures 8 and 9 as well as Scheme 9).

Another path variant starts also from **26**. A coordination change from Zn bound carbon to the carbonyl oxygen can occur (formation of **30**; Scheme 9). Water is not involved in this reaction step. It remains between the two ammonia ligands and stabilizes the transition state **29(ts)** by means of an hydrogen bond to the carbonyl oxygen (d = 1.758 Å). The structure **29(ts)** is a high strained species. The CZnO angle is 62.5°, and the distance of the breaking ZnC bond is 2.363 Å and 2.058 Å for the forming ZnO bond. The activation barrier for the coordination change is $\Delta\Delta G$ = 48.2 kJ/mol. **29(ts)** relaxes to give the intermediate **30** with Zn bound carbonyl oxygen. In this structure, the carbon backbone is not perpendicular to the plane spanned by the ammonia ligands as expected for intermediates with Zn bound oxygens.[52,60,61] The ZnOCC dihedral angle is 31.2°. The reason for this fact is an interaction between the terminal carbon of the new double bond and an ammonia hydrogen (d = 2.374 Å). The second-order perturbation theory analysis determined $E(2)$ = 17.6 kJ/mol for this interaction. Further, this carbon has a charge of −0.66 determined from the natural population analysis which leads to a coulomb attraction to the ammonia hydrogen (natural charge 0.45). The Gibbs free energy for **30** is $\Delta G = -127.0$ kJ/mol and is therefore $\Delta\Delta G$ = 10.9 kJ/mol less stable than **26** (Figure 8).

The next step is a new alignment of the water molecule in **30** to form the water encounter complex **31**, which is preconfigurated to shift one water hydrogen via the transition state **32(ts)** to the methylene group similar to the transition states **10(ts)** and **17(ts)** (Scheme 7). For **31** exists an attraction between one water hydrogen and the terminal carbon of the double bond based on $\pi-$CC orbital and σ^*-HO overlay ($E(2) = 54.5$ kJ/mol), comparable to the water encounter complex **9**.

32(ts) is a 6-membered concerted TS with trigonal bipyramidic geometry (Figure 9). The water oxygen is located at one axial tip and 2.035 Å remote of zinc (breaking ZnO bond $d =$ 1.990 Å). The shifted hydrogen is 1.366 Å remote of the attacked carbon. Only $\Delta\Delta G_a = 32.6$ kJ/mol is needed to overcome the activation barrier. No further intermediates were found. **32(ts)** relaxes directly into the product complex **33**. It consists of acetone and free initial hydroxide complex **5**. Acetone is placed between two ammonia ligands with its carbonyl oxygen and is stabilized by two hydrogen bonds ($d =$ 1.987 Å). This reaction path variant via **32(ts)** is the only one to obtain acetone directly without the preceding formation of the enol form.

A further possibility is the following: As discussed for the key intermediate **8**, water can attack the Zn bound carbon atom starting with intermediate **26**. As in **22(ts)**, a concerted 4-membered TS will be expected. However, scanning of the potential hypersurface indicates another reaction mechanism. If the water hydrogen approximates to the carbon, the ZnC bond breaks. Instead of forming the hydroxide complex, the carbonyl oxygen coordinates and a noncoordinated methylene group is generated (structure **31**). Accordingly, the reaction path follows as described above.

Without the new alignment of the water molecule, the zinc bound oxygen of intermediate **30** can immediately be attacked (Scheme 9). The resulting transition state **34(ts)** is a concerted 4-membered TS similar to **22(ts)** (Scheme 8). **34(ts)** has a distorted trigonal bigyramidic geometry (Figure 9). The water oxygen is 1.988 Å remote of zinc. The OZnO angle is 65.3° so that the OHO can be 148.6°. The activation barrier for this step is $\Delta\Delta G_a = 42.1$ kJ/mol and as a consequence 10.5 kJ/mol higher than for **32(ts)** (Figure 8). **34(ts)** relaxes to give the product complex **35**. It consists of **4-i** and **5**. Like all other product complexes, it is stabilized by hydrogen bonds as shown in Figure 9.

The last path variant for the reaction of allene and the ammonia model of carbonic anhydrase described here is the decomposition of the key intermediate **8** back to the starting components **1**, **5**, and water (Scheme 10). For this alternative, a hydrogen of the attacking water must be shifted to the hydroxide group and not to the methylene group. Structure **36** is the corresponding water encounter complex. Water is stabilized by hydrogen bonds to the hydroxide group and two ammonia ligands. With $\Delta G = -61.1$ kJ/mol, it is the second stablest water encounter complex with intermediate **8**. A transition state for hydrolysis **37(ts)** was hard to find. Gibbs free energy for **37(ts)** is $\Delta G = 141.0$ kJ/mol and thus higher than the initial attack to allene. As a consequence, the activation barrier is $\Delta\Delta G = 202.1$ kJ/mol (Figure 8). This path variant is most improbable. A new water molecule and the starting compound, allene, come into existence, and the zinc hydroxide complex is regenerated. The product complex (or starting material, depending on the point of view) is structure **38** (Figure 9).

Conclusions

From this investigation, we conclude that allene, which is isoelectronic with CO2, should have the capability to interact with models of carbonic anhydrase in a manner which will allow the inexpensive transformation of this abounding cumulene. Application of high level DFT calculations leads to a manifold of very plausible reaction paths. The rate-determining step for all variants is the initial nucleophilic attack of the hydroxy group of the zinc complex at the C(2) of the allene with the decomposition reaction (regeneration of the starting components; cf. Scheme 10) being the only exception. Energy relationships indicate that this variant can be excluded. Both the attacks at the central and/or the terminal allene carbons can proceed on a lower energetic level. Which one will be more successful? The important reaction steps via a 4-membered cyclic transition structures differ only by about $\Delta\Delta G = 15$ kJ/mol; therefore, the attack at the central carbon and the selective formation of **8** is slightly preferred. The water addition to the intermediate **8a** induces a hydrogen shift to the zinc bound central carbon and is characterized by a relatively high activation barrier ($\Delta\Delta G_a = 104.8$ kJ/mol). The product of this pathway is allyl alcohol.

The other reaction path which starts with the nucleophilic attack on the central allene carbon was investigated thoroughly. The key structure for this reaction is the intermediate **8** after surmounting the initial transition state **7(ts)**. From that structure, a variety of interesting reaction paths have been detected. Our calculations indicate that the variants with the lowest activation barriers are the water attacks at the free methylene group via 6-membered cyclic TSs (structure **10(ts)** and **17(ts)**). The rotation of the hydroxide group before the water attack does not lead to great differences for the energetic and structural properties. Therefore both path variants are probable. The activation barrier for the hydrogen shift via the 4-membered cyclic TS **22(ts)** to the zinc bound terminal carbon is nearly as high as for initial nucleophilic attack. This attack is likely negligible. Alternatively, a water catalyzed hydrogen shift from the hydroxide to the methylene group via the 6-membered cyclic TS **25(ts)** can proceed in the propenole moiety. Even though further reaction paths arise out of the proceeding intermediate, the activation barrier speaks against such an alternative. Water can directly attack the carbonyl oxygen over the 6-membered cyclic TS **27(ts)** or a coordination change from zinc bound carbon to zinc bound oxygen occurs over the 4-membered cyclic TS **29(ts)**. After the coordination change, water can attack the zinc bound oxygen. The products from all of these paths are isomers of propene-2-ol. The only reaction path from which acetone is directly generated is the hydrogen shift to the newly formed methylene group over the 6-membered cyclic TS **32(ts)** after the coordination change.

(54) Liang, J. Y.; Lipscomb, W. N. *Biochemistry* **1987**, *26*, 5293–5301.
(55) Lipscomb, W. N. *Annu. Rev. Biochem.* **1983**, *52*, 17–34.
(56) Weinhold, F.; Glendening, E. D. *J. Comput. Chem.* **1998**, *19*, 593–609.
(57) Weinhold, F.; Glendening, E. D. *J. Comput. Chem.* **1998**, *19*, 610–627.
(58) Weinhold, F.; Glendening, E. D.; Badenhoop, J. K. *J. Comput. Chem.* **1998**, *19*, 628–646.
(59) Wiberg, K. B. *Tetrahedron* **1968**, *24*, 1083–1096.
(60) Bertran, J.; Sola, M.; Lledos, A.; Duran, M. *J. Am. Chem. Soc.* **1992**, *114*, 869–877.
(61) Schenk, S.; Notni, J.; Köhn, U.; Wermann, K.; Anders, E. *Dalton Trans.* **2006**, 4191–4206.

Due to the clear-cut results, currently experimental examinations of the reaction of allene with synthesized CA model systems are in progress. Experiments are based on zinc hydroxide complexes with azamacrocylic ligands inspected with Raman spectroscopy.[62−64] Zinc catalysis of the "worst case" allene ($\Delta\Delta G_a$ = 123.9 kJ/mol) in comparison with ketene ($\Delta\Delta G_a$ = 36.6 kJ/mol and, respectively, $\Delta\Delta G_a$ = 75.9 kJ/mol dependent on the attacked bond) and carbon dioxide ($\Delta\Delta G$ = 55.6 kJ/mol), appears to be feasible as an efficient method adding value to a cheap byproduct of industrial process.

Acknowledgment. Financial support by the Deutsche Forschungsgemeinschaft is gratefully acknowledged.

Supporting Information Available: Gas phase and solvent corrected energies as well as geometries for all structures reported. This material is available free of charge via the Internet at http://pubs.acs.org.

JO801358M

(62) Notni, J.; Görls; H.; Anders, E. *Eur. J. Inorg. Chem.* **2007**, *7*, 985–993.
(63) Kimura, E.; Shiota, T.; Koike, T.; Shire, M.; Kodama, M. *J. Am. Chem. Soc.* **1990**, *112*, 5805–5811.
(64) Uhlemann, U.; Schmitt, M.; Oehme, K.-L.; Notni, J.; Anders, E.; Popp, J. *J. Raman Spectrosc.* **2006**, *37*, 442–446.